Re-entrant kinetic arrest and elasticity of concentrated suspensions of spherical and nonspherical repulsive and attractive colloids

Cite as: J. Chem. Phys. **134**, 014503 (2011); https://doi.org/10.1063/1.3509393
Submitted: 03 August 2010 • Accepted: 12 October 2010 • Published Online: 04 January 2011

Ryan C. Kramb, Rui Zhang, Kenneth S. Schweizer, et al.

Re-entrant kinetic arrest and elasticity of concentrated suspensions of spherical and nonspherical repulsive and attractive colloids

Ryan C. Kramb,[1,2,a)] Rui Zhang,[2,3] Kenneth S. Schweizer,[1,2,3] and Charles F. Zukoski[1,2,3,b)]

[1]*Department of Chemical and Biomolecular Engineering, University of Illinois, Urbana, Illinois 61801, USA*
[2]*Frederick Seitz Materials Research Laboratory, University of Illinois, Urbana, Illinois 61801, USA*
[3]*Department of Materials Science, University of Illinois, Urbana, Illinois 61801, USA*

(Received 3 August 2010; accepted 12 October 2010; published online 4 January 2011)

We have designed and studied a new experimental colloidal system to probe how the weak shape anisotropy of uniaxial particles and variable repulsive (Coulombic) and attractive (van der Waals) forces influence slow dynamics, shear elasticity, and kinetic vitrification in dense suspensions. The introduction of shape anisotropy dramatically delays kinetic vitrification and reduces the shear elastic modulus of colloidal diatomics relative to their chemically identical spherical analogs. Tuning the interparticle interaction from repulsive, to nearly hard, to attractive by increasing suspension ionic strength reveals a nonmonotonic re-entrant dynamical phase behavior (glass–fluid–gel) and a rich variation of the shear modulus. The experimental results are quantitatively confronted with recent predictions of ideal mode coupling and activated barrier hopping theories of kinetic arrest and elasticity, and good agreement is generally found with a couple of exceptions. The systems created may have interesting materials science applications such as flowable ultrahigh volume fraction suspensions, or responsive fluids that can be reversibly switched between a flowing liquid and a solid nonequilibrium state based on *in situ* modification of suspension ionic strength. © *2011 American Institute of Physics*. [doi:10.1063/1.3509393]

I. INTRODUCTION

Great excitement has been recently generated by computer simulation studies which reveal unique clustering arrangements and the possibility of novel forms of long range order based on particles with anisotropic shape and/or interaction potentials.[1–5] In parallel, there have been numerous reports of the synthesis of nonspherical nanoparticles and colloids.[4–15] Simulations suggest that when chemically heterogeneous or "patchy" particles experience a limited number of attractive interactions there is a large reduction of the critical temperature for liquid-gas type of phase separation.[1] In addition, microscopic theory and simulation find particle shape anisotropy can strongly modify the onset of nonequilibrium glassy states including a striking nonmonotonic dependence of the vitrification volume fraction on the degree of anisotropy of dumbbells,[16–20] triatomics,[21] spherocylinders,[21,22] ellipsoids-of-revolution,[23,24] and more complex shapes.[25,26] Similar nonmonotonic variation has been observed for the jamming packing fraction of hard granular ellipsoids and spherocylinders.[27–29] Going beyond the hard particle paradigm, there has also been experimental and theoretical work on kinetic arrest in soft spherical particle systems such as many-arm star polymers,[30] crosslinked microgels,[31–33] and block copolymer micelles.[34]

At the moment, simulation and theory are well ahead of experimental studies in advancing understanding of suspensions of structurally and/or chemically anisotropic particles. Experimental advances have been limited by two major hurdles. First, synthetic methods for producing large quantities of uniform anisotropic colloids or nanoparticles are in their infancy. Because the synthetic methods result in particles that are not uniform and/or are relatively scarce, exploration of the large array of configurations and bulk properties associated with shape and interaction energy anisotropy have been limited. Until methods are developed that consistently produce uniform particles with reliable anisotropy in large quantities, progress will be slow. Second, even when such particles can be synthesized in large quantities, methods for characterizing the strength of the anisotropic interactions are poorly developed.

Progress in developing a predictive theoretical understanding requires accounting for shape and/or interaction energy anisotropy in ways that are mathematically tractable. Recent advances have been reported for the slow glassy dynamics aspects of the problem based on the microscopic ideal mode coupling theory (MCT) framework[17] for shape anisotropic, but chemically homogeneous, hard particles. Specifically, MCT has made predictions for the influence of aspect ratio on the ideal kinetic glass transition of uniaxial hard core particles that accounts for both center-of-mass (CM) and orientational degrees of freedom.[16,20,23] Quantitative results are possible due to the availability of theoretical methods to describe equilibrium structure of isotropic fluids. However, the full ideal MCT of nonspherical particles[16,23] is sufficiently complex that it has seen limited application to the vast array of particle shapes and pair potentials now possible to realize experimentally. Moreover, at high enough volume fractions,

a)Present address: Air Force Research Laboratory, Wright-Patterson Air Force Base, Ohio 45433, USA.
b)Electronic mail: czukoski@illinois.edu.

the long time dynamics is not properly described since the MCT nonergodicity transition is an artifact of neglecting nonperturbative, large amplitude hopping processes which restore ergodicity.[17,35–38]

The rare activated processes not captured in ideal MCT are accurately described by the nonlinear Langevin equation theory (NLE) for spherical particles where ergodicity is restored via barrier hopping.[35,39,41] If hopping is ignored, the NLE theory reduces to a conceptually and mathematically simplified (and cruder) "naïve" version of ideal MCT (NMCT)[39,40,42] which also predicts an ideal glass transition at a critical volume fraction ϕ_c. However, ϕ_c does not denote literal arrest but rather a dynamic crossover to an even slower form of dynamics controlled by activated barrier hopping. Recently, the NLE and NMCT theories have been extended to treat coupled translational and rotational glassy dynamics of uniaxial particles within an interaction site representation.[20] However, this approach is not yet able to predict mechanical properties. The only theory presently available that has addressed nonspherical shapes, variable repulsive and attractive pair potentials, and shear elasticity is the CM versions of the NMCT and NLE approaches.[19,21,22,25,26] Physically, the CM theory assumes translational motion controls confining force relaxation and cage escape, a simplification that has been shown to be reliable for the modestly anisotropic particles of present experimental interest.[20,43]

Here we report results of a coordinated experimental and theoretical study of kinetic arrest and shear elasticity of dense suspensions of weakly anisotropic particles composed of fused spheres of equal size ("dicolloids") and their spherical analog. By controlling suspension ionic strength, the interparticle forces can be tuned from repulsive to a system with weak or relatively strong attractive forces. This allows us to address the following questions: (1) How does particle shape modify the kinetic arrest volume fraction as a function of ionic strength? (2) Does the dramatic glass-to-fluid-to-gel dynamic "re-entrancy" phenomenon observed for mixtures of hard sphere colloids and nonadsorbing small polymers[44,45] also occur for more complex spherical particles as a function of ionic strength? (3) How does nonspherical particle shape modify the re-entrancy phenomenon? (4) How does the shear modulus of hard and sticky spheres and dicolloids vary with volume fraction and interaction potentials, and what is the role of particle shape? (5) Can any universality be identified for the shear elastic response? (6) Is there a connection between the onset of activated dynamics at ϕ_c and the jamming volume fraction ϕ_{RCP}? These questions have been very recently studied by us in a brief Letter focused on colloids that interact solely via repulsive forces.[43] In this article, the repulsive particles are studied in greater depth, and the new question of the role of variable attractive forces is addressed in detail.

The remainder of the article is structured as follows. The CM-NMCT and NLE theories are briefly reviewed in Sec. II. The experimental aspects, including particle synthesis and characterization, computation of pair potentials, and rheological measurements, are the subject of Sec. III. Section IV presents our experimental results and their quantitative comparison to theoretical predictions, and discusses the physics. The paper concludes in Sec. V with a brief summary and future outlook.

II. THEORY

The dynamical theory we apply has been developed recently[19,22] and is discussed in depth in the literature. Here we summarize only the elements relevant to our present work. Rigid, nonspherical particles are described in the interaction site model representation.[19,46] The intermolecular site–site pair correlations and static structure factors are the key input to the dynamical theory and are computed using the reference interaction site model (RISM) of Chandler and Andersen.[46] For rigid objects composed of symmetry-equivalent units (such as homonuclear dicolloids) a single scalar integral equation describes packing structure which in Fourier transform space is given by

$$h_{ss}(k) = \omega_{ss}(k)C_{ss}(k)\omega_{ss}(k) + \rho_s\omega_{ss}(k)C_{ss}(k)h_{ss}(k). \quad (1)$$

Here ρ_s is the site number density, $h_{ss}(k)$ is the Fourier transform of the intermolecular site–site total correlation function $h_{ss}(r)=g_{ss}(r)-1$, $C_{ss}(k)$ is the Fourier transform of the intermolecular site–site direct correlation function, and $\omega_{ss}(k)$ the intramolecular structure factor. We employ the site–site Percus–Yevick (PY) closure approximation:[46,47]

$$C_{ss}(r) = (1 - e^{\beta U(r)})g_{ss}(r), \quad (2)$$

where $U(r)$ is the noncontact interparticle site–site potential and $\beta \equiv (k_B T)^{-1}$ is the inverse thermal energy. Equation (2) applies outside the distance of closest approach between two sites (D), and inside the hard core the exact impenetrability constraint is enforced: $g_{ss}(r)=0$, $r<D$. The site–site total density fluctuation structure factor is

$$S_{ss}(k) = \omega_{ss}(k) + \rho_s h_{ss}(k) = \frac{1}{\omega_{ss}^{-1}(k) - \rho_s C_{ss}(k)}. \quad (3)$$

Its CM analog, which is the key input to the dynamic theory employed in this article, is[19]

$$S_{CM}(k) = \frac{S_{ss}(k)}{\omega_{ss}(k)} = 1 + \rho h_{CM}(k) = \frac{1}{1 - \rho C_{CM}(k)} \quad (4)$$

with $\rho=\rho_s/N$ ($N=2$ for dicolloids, $N=1$ for spheres) and

$$C_{CM}(k) = N\omega_{ss}(k)C_{ss}(k), \quad (5)$$

$$h_{CM}(k) = \frac{N}{\omega_{ss}(k)}h_{ss}(k). \quad (6)$$

The intraparticle structure factor of a sphere is unity, and for a rigid dicolloid (bond length b): $\omega_{ss}(k)=1+(kb)^{-1}\sin(kb)$.

The CM-NLE theory describes the scalar displacement of a particle from its initial position, $r(t)$, which obeys the following closed nonlinear stochastic equation in the overdamped limit:[39–41]

$$\zeta_s \frac{\partial r(t)}{\partial t} = \frac{\partial F_{eff} - (r(t))}{\partial r(t)} + \delta f(t), \quad (7)$$

where $\zeta_s=k_BT/D_s$ is the short time friction constant, the random thermal force satisfies $\langle \delta f(0)\delta f(t)\rangle = 2k_BT\zeta_s\delta(t)$, and D_s is the CM short time self-diffusion constant. The latter is well

understood for hard sphere suspensions,[39] but not for dicolloids. The key quantity in Eq. (7) is the dynamic free energy, $F_{\rm eff}(r(t))$, which describes within a local equilibrium dynamic density functional framework the effect of the surrounding particles on a tagged particle. In terms of CM variables it is given in units of k_BT by[39,40]

$$F_{\rm eff}(r) = -3\ln(r) - \int \frac{d\vec{k}}{(2\pi)^3} \frac{\rho C_{\rm CM}^2(k) S_{\rm CM}(k)}{1 + S_{\rm CM}^{-1}(k)} \times \exp\left\{-\frac{k^2 r^2}{6}(1 + S_{\rm CM}^{-1}(k))\right\}. \quad (8)$$

Minimization of Eq. (8) with respect to r can be shown to be equivalent to solving the NMCT self-consistent equation for the ensemble-averaged long time limit of the particle mean square displacement, known as localization length, $r_{\rm loc}$, given by[39,42]

$$r_{\rm loc}^{-2} = \frac{1}{9} \int \frac{d\vec{k}}{(2\pi)^3} \rho k^2 C_{\rm CM}^2(k) S_{\rm CM}(k) \times \exp\left\{-\frac{k^2 r_{\rm loc}^2}{6}\left(1 + S_{\rm CM}^{-1}(k)\right)\right\}, \quad (9)$$

which relates the tendency for localization to the strength of the mean square forces exerted on a particle by its surroundings; the latter are determined by material-specific structural correlations and interactions.[48] As volume fraction increases, $r_{\rm loc}$ discontinuously changes from infinity (a fluid) to a finite value at a critical volume fraction, ϕ_c, which defines the onset of transient localization (crossover to activated dynamics) and a qualitative change of $F_{\rm eff}(r)$ to a form characterized by a localization well and barrier.

Beyond ϕ_c the mean first passage or barrier hopping time in the high friction overdamped (diffusive barrier crossing) limit follows from Kramers theory:[39]

$$\frac{\tau}{\tau_s} = \frac{2\pi}{\sqrt{\tilde{K}_0 \tilde{K}_B}} \exp\left(\frac{F_B}{k_B T}\right), \quad (10)$$

where $\tau_s = D^2\zeta_s/k_BT$ (site diameter D), F_B is the barrier height, and $\tilde{K}_0$ and $\tilde{K}_B$ are the absolute magnitudes of the well and barrier harmonic curvatures in units of k_BT/D^2, respectively. The hopping time is closely related to the alpha relaxation time of glassy materials,[35] and we adopt here as a measure of the experimental mean stress relaxation time. Quantitative "prefactor" differences between the hopping and stress relaxation times are expected to result in very modest quantitative shifts of computed kinetic glass transition volume fractions. Note Eq. (10) depends on the ratio τ_s/τ_0 which is greater than unity due to short time dissipative dynamics (where τ_0 is the dilute suspension limit elementary Brownian time). For example, for hard spheres at a volume fraction of 0.5, $\tau_s/\tau_0 \sim 5$.

NMCT in conjunction with a standard Green–Kubo formula and projection-factorization simplifications allows calculation of the glassy elastic shear modulus[49,50]

$$G' = \frac{k_BT}{60\pi^2} \int_0^\infty {\rm dk} \left\{k^2 \frac{d}{dk} \ln(S_{\rm CM}(k))\right\}^2 \times \exp\left\{-k^2 r_{\rm loc}^2 / 3 S_{\rm CM}(k)\right\}. \quad (11)$$

The shear modulus is entirely determined by the CM localization length and structure factor. In principle, Eq. (11) literally applies only in the ideal glass state of MCT. We employ it here as a sensible approximation of the physically relevant *intermediate time* plateau of the stress relaxation function associated with the transiently localized state which continues to exist even in the presence of activated hopping at long times.

III. EXPERIMENTAL

A. Synthesis and characterization

Particles were synthesized using a modified version of the seeded emulsion polymerization technique of Mock *et al.*[9] The seeds used to make the spherical particles contained no divinylbenzene (DVB) crosslinker, while the seeds used for the dicolloids contained 2% DVB (Aldrich, 55% mixture of isomers tech. grade) by weight. The seeds were otherwise identical and synthesized by surfactant [sodium dodecyl sulfate (SDS)] stabilized polymerization of styrene. Both sets of seed particles were synthesized in 5 l round bottom flasks immersed in a constant temperature water bath. A poly(tetraflouroethylene) coated blade attached to a rotating glass bar was used for stirring. Initially 3.75 g of SDS was dissolved in 3000 ml of deionized water. The water was allowed to reach a steady state temperature of 80 °C and 350 ml of styrene monomer (Sigma-Aldrich, 99% purity grade) was added. For the dicolloid seeds, the DVB was dissolved into the styrene added in this step. The solution was stirred at 80 °C for 1 h at a vigorous speed. Then, 11.7 g of potassium persulfate initiator (Fisher Scientific 99.5% purity grade) dissolved in 560 ml of water was added, and the reaction was allowed to proceed for 24 h. The resulting seed particles were nearly identical: 210 nm in diameter (±3.2 nm) for the sphere seeds, 211 nm (±1.5 nm) for the dicolloid seeds.

The particles were then swollen with additional styrene monomer at a mass ratio of 2:1 (swelling styrene to seed particle mass). For this swelling step, 880 ml of the seed particle solution was poured into a 5 l round bottom flask along with 620 ml of a 0.1 M potassium hydroxide (KOH) solution, 2.5 g of SDS, and 2.4 g of azobisisobutyronitrile dissolved in 130 ml of additional styrene. The flask was stirred at room temperature for 24 h. When the swelling was complete, 5 ml of methacrylic acid and 40 g of hydroquinone dissolved in 500 ml of the KOH solution were added to the vessel and the temperature was elevated to 70 °C. The reaction proceeded for 24 h.

The resulting final particles are shown in the inset of Fig. 1. The spheres have a mean diameter of 270 nm (±1.6 nm), while the dicolloids had a mean long axis length of 330 nm (±2.2 nm) and a mean short axis length of 250 nm (±2.1 nm) as measured by scanning electron microscopy (SEM Hitachi S4700). The aspect ratio of the dicolloids, length divided by sphere diameter, is thus L/D=1.3. In addition to SEM measurements, the particle diffusivity was determined using dynamic light scattering (Brookhaven Instruments bench top fiber optic quasielastic light scattering) and found to be consistent with particles of the SEM size

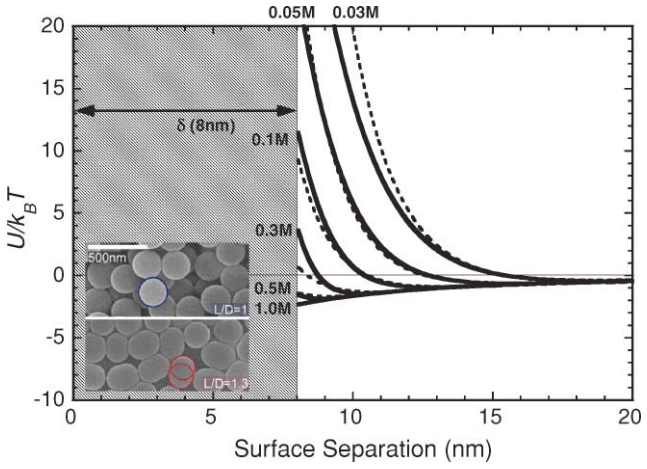

FIG. 1. Calculated particle pair interaction energies including full van der Waals and electrostatic forces (solid curves), and their double Yukawa fits (dashed curves). Inset: SEM micrographs of the sphere and dicolloid particles.

indicating no aggregation occurred during processing. After synthesis the particles are dialyzed against a polyethylene glycol (PEG) (20 000 molecular weight, Sigma) in deionized water solution with approximately 30–50 g of PEG and 3 l of water to remove unwanted electrolytes and oligomers. The dialysis process also concentrates the particles by drawing water out of the dialysis tubes. Once the volume fraction of particles in the tube reached approximately 0.35–0.40, 15–25 ml portions of the solution were transferred to a 50 ml centrifuge tube containing 0.338 g of the surfactant $C_{12}E_6$. The $C_{12}E_6$ coats the surface of the particles and results in a bound steric layer approximately 4 nm thick.[51] This layer sets the minimum surface-to-surface separation where the van der Waals forces from the polystyrene cores are operative to be 8 nm. By working with particles of diameter D=200–300 nm, the maximum well depth at contact of the surfactant coated particles is estimated to be 1–5k_BT. Finally, a bulk solution of either 0.1, 0.5, 1.0, or 5.0 M sodium chloride (Fisher Scientific, crystalline) dissolved in deionized water was added such that the final concentration of $C_{12}E_6$ was 0.03 M, the ionic strength of the solution varied from 0.03 to 1.0 M, and the total volume in the tube was 25 ml. The tubes were then centrifuged at 6000 rpm (∼4000 g) for 1 h intervals and the supernatant removed until further centrifuge cycles produced no removable supernatant. The volume fraction at this stage ranged from 0.55 to 0.65, and served as the bulk solution to be diluted for rheological experiments.

B. Interaction potentials and physical regimes

To perform a quantitative, *no adjustable parameter* comparison between experiment and theory, the particle interaction potentials are required. Standard Derjaguin and Landau, Verwey and Overbeek (DLVO) calculations were performed using a van der Waals Hamaker constant of 3.1kT with a minimum polystyrene (PS) intersurface separation distance of 8 nm (twice the $C_{12}E_6$ surfactant thickness), electrophoretically derived electrostatic surface potentials of –20, –16, –12 and –8, –3, and –1 mV for [I]=0.03, 0.05, 0.1, 0.3, 0.5, and 1.0 M, respectively, and a Debye–Huckel screening length set by [I]. Surface potentials were taken to be independent of particle shape. The resulting site–site potentials are shown in Fig. 1. An effective hard diameter (and corresponding effective volume fraction[52]) is estimated as the distance at which the repulsion is 1kT. By varying ionic strength, the potential can be tuned from very short range repulsive (nearly "hard") to a "mixed" potential at [I]=0.3 M which has an attractive noncontact minimum of ∼1.5kT, to a relatively strongly attractive at contact system with a ∼3kT well depth at [I]=1.0 M.

Of course, there must be some quantitative uncertainties in the potentials of Fig. 1 which can arise from multiple real world sources such as: surfactant and solvent dielectric constant mismatch, thin solvation layers of water around the particles, and uncertainty of surfactant layer thickness due to nonideal structure. These effects are expected to have little consequences at low ionic strengths where the particles are strongly repulsive, the regime studied in prior work.[43] However, at high ionic strengths the depth and form of the attractive component of $U(r)$ is more sensitive to these complications, especially surfactant layer thickness and structure. This limitation should be kept in mind when theory and experiment are quantitatively compared in Sec. IV since attractive forces can have dramatic consequences (e.g., gel versus glass[44]).

By varying ionic strength, very different physical behavior is expected to be accessed. At low ionic strength (<0.01 M), the surface charges are not significantly screened and the particles experience long range repulsive forces. These conditions prevent dense packing and can encourage crystalline ordering at low concentrations. The (slightly) soft repulsion also blurs the differences between the two particle shapes.[53] Our goal is to investigate particles that interact via nearly hard core repulsive plus variable attractive interactions where shape differences will be accentuated. This motivated our choice to work at higher salt concentrations. At ionic strengths of 0.03–0.1 M, the surface charges are moderately screened. The Debye screening length is ∼1–2 nm, and the resulting pair potentials resemble those of hard particles but with slightly larger dimensions than the surfactant coated particles. At ionic strengths near 0.3 M where the Debye screening length is 0.5 nm or smaller, a weak attractive minimum in the pair potential emerges. At the highest ionic strengths (>0.5 M), essentially all surface charges are screened and an attractive well depth of 2–3kT is present resulting in rapid particle aggregation and, at high enough volume fractions, physical gelation.

Confirmation that we have reached approximate "hard" conditions at 0.03 M is made by measuring the suspension viscosity of spheres and dicolloids as a function of ionic strength at a volume fraction of 0.3. Figure 2 shows the results, and one sees that at low to moderate volume fractions (below ϕ_c) where transient localization does not occur, repulsions and attractions will both increase viscosity above the hard interaction values.[54] Above ϕ_c the attractions have been shown to result in viscosities below the hard interaction values.[55] We view the viscosity minimum in Fig. 2 as

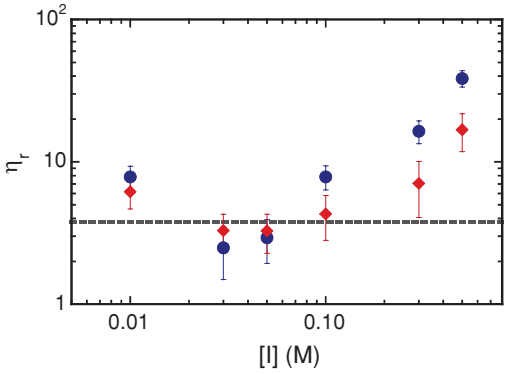

FIG. 2. Low shear rate viscosities of suspensions of sphere (blue) and dicolloid (red) particles at ionic strengths from 0.01 to 0.5 M and $\phi \approx 0.30$. A minimum is reached at ~0.02–0.05 M indicating approximately hard core interactions. Hard sphere viscosity at ϕ=0.3 is shown as a dashed line (Ref. 65).

indicating when the particles are optimally hard, which occurs [I]=0.02–0.05 M.

For computational convenience in the theoretical analysis, we have fit the numerically determined interaction pair potentials with a double Yukawa function:

$$\frac{U(r)}{k_B T} = -\frac{AD}{r}\exp\left(-\frac{D}{\lambda_a}\left(\frac{r}{D}-1\right)\right) + \frac{BD}{r}\exp\left(-\kappa D\left(\frac{r}{D}-1\right)\right), \quad (12)$$

where A is the contact value of the truncated van der Waals attraction ($2.3kT$) and λ_a=0.025D. The parameter B is set at the contact value of the electrostatic repulsion based on the zeta potential as measured by electrophoresis, and the screening length is $1/\kappa$ where κ is the Debye–Huckel parameter. The parameters used in the calculations are listed in Table I. The accuracy of the Yukawa fits is illustrated in Fig. 1.

C. Rheological measurements

Rheological measurement of viscosities and frequency-dependent storage and loss moduli were obtained using a Bohlin C-VOR rheometer with a cup and bob geometry. The bob is made from roughened titanium with a diameter of 14 mm and a gap size of 0.7 mm with a sample volume of 3 ml. Temperature was maintained with a constant temperature water bath at 30±0.5 °C. This temperature was maintained during preparation steps and was chosen in order to stay above the freezing point of the surfactant (27 °C).

TABLE I. Parameters used for analytic Yukawa fits of the numerically computed pair potentials.

Ionic strength (M)	B (k_BT)	κ (1/Å)
0.03	79	0.06
0.05	32	0.07
0.1	14	0.08
0.3	3.6	0.093
0.5	1.1	0.1
1.0	<0.1	0.2

The protocol employed for the viscoelastic experiments is as follows. First, 3.2 ml of the highly concentrated bulk suspension in the centrifuge tube is transferred to the rheometer cup. Then 0.2 ml is removed and the mass measured in a 20 ml scintillation vial. The vial was then placed in an oven at 110 °C to remove water from the solution. The dried weight was measured after 24 h and the weight fraction of polystyrene was calculated (taking into account remaining salt in the vial). This was converted into a volume fraction using reported densities of polystyrene (1.05 g/ml), and measured values of water containing NaCl. The remaining 3 ml of sample in the cup was used for the mechanical experiments. A solvent trap is placed around the shaft of the bob limiting water evaporation and volume fraction increases during experiment runs. However, even with the solvent trap in place, total experimental time longer than 30 min for any one sample was avoided as changes in mechanical properties were observed after this length of time. The sample is presheared at a rate of 50 s^{-1} for 2 min and data collection began 10 s after the preshear step. The elastic and viscous moduli were measured as a function of applied stress at a frequency of 1 Hz for the first experiment for each sample. The modulus measured in the plateau of this stress sweep is the value reported for each volume fraction in the figures of Sec. IV. Plateau moduli were found to be reproducible, within experimental error and accounting for increases in volume fraction due to solvent evaporation, by occasionally repeating experiments at the end of each run.

After the first set of experiments at a specified ionic strength, the bob was cleaned and any sample remaining on the bob discarded. However, the sample remaining in the cup was kept in order to conserve material and allow an adequate number of volume fractions to be studied. Approximately 2.5–2.8 ml of the previous sample typically remained in the rheometer cup after this initial experiment. To this, an additional 0.1 ml of a solution containing 0.03 M $C_{12}E_6$ and dissolved NaCl (at the same ionic strength as the sample already in the cup) was added. Finally, a small amount of the bulk particle solution from the centrifuge tube was added until the total volume in the cup again reached 3.2 ml. The process for measuring volume fraction was repeated for this sample. The effect of this material-conserving dilution process was that the volume fraction for the new sample decreased by about 0.01–0.02% from the previous sample. The entire process was then repeated again, lowering the volume fraction each time, until a plateau in the elastic modulus could not be observed at even the lowest stresses of the stress sweep experiment discussed below.

IV. RESULTS AND DISCUSSION

For each ionic strength, a stress sweep is performed at fixed oscillation frequency and the elastic and viscous moduli (G', G'') are measured. Unless stated otherwise, all results are based on an oscillation frequency of 1 Hz. At small stresses, a constant linear response modulus is observed. All subsequent G' and G'' refer to this linear response value which is used to determine the quiescent relaxation time and kinetic arrest diagram.

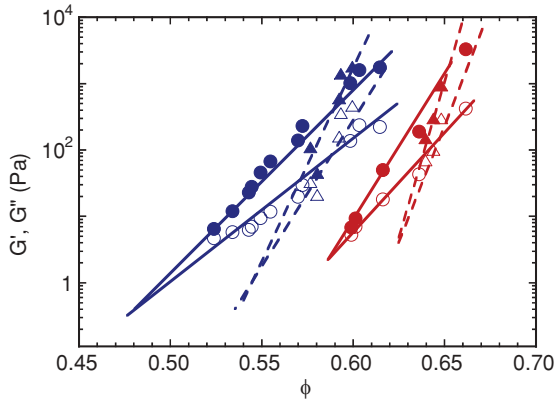

FIG. 3. Procedure for determining ϕ_g. $G'(\phi)$ (solid points) and $G''(\phi)$ (open points) are plotted for S (blue) and sDC (red) at ionic strengths of 0.03 M (circles) and 0.3 M (triangles) and 1 Hz.

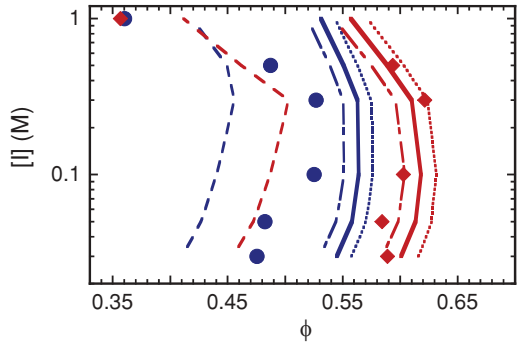

FIG. 5. Dynamical state diagram showing ϕ_g for S (blue filled circles) and sDC (red filled diamonds). Experimental ϕ_g is shown as points. NMCT theory calculations of ϕ_c shown as dashed curves. NLE theory calculations of the kinetic ϕ_g are shown using $\tau=1$ s (dash-dot), 2π s (solid), 50 s (dot).

A. Relaxation times and kinetic arrest

In the Maxwell model spirit, a relaxation time is defined from the condition $G'=G''$. For the larger volume fractions studied, this relaxation time is longer than the experimental time and the system displays solidlike properties. As a result we use this as the criterion for determining the experimental kinetic glass transition volume fraction (ϕ_g). The procedure for locating the volume fraction where $G'=G''$ at 1 Hz (corresponding to a relaxation time of 2π s) is outlined in Fig. 3 where G' and G'' are plotted at ionic strengths of 0.03 and 0.3 M. The $G'(\phi)$ and $G''(\phi)$ data are fit to exponential functions and (mildly) extrapolated to the condition $G'=G''$. Limited frequency sweeps were made to investigate the frequency dependence of the modulus. As shown in Fig. 4, the elastic moduli are indeed solidlike, being nearly independent of frequency over the range probed. For all values of the elastic modulus reported below, the experimental frequency of 1 Hz falls within the glassy or gel-like plateau.

Figure 5 shows the experimental nonequilibrium phase diagram in the representation of ionic strength versus volume fraction for spheres and dicolloids at the five ionic strengths. With the exception of the 1.0 M samples, the most obvious feature is the dramatic increase of the kinetic arrest volume fractions for the dicolloid. Both spheres and dicolloids show a nonmonotonic variation of the kinetic glass volume fraction with ionic strength, the signature of "re-entrancy".[44,45,56–58] Specifically, the kinetic arrest transition boundary first shifts to higher volume fractions with increasing ionic strength, which is partially a consequence of a reduced effective hard core diameter as Coulomb repulsion is better screened, and partially a consequence of the increasing presence of weak attractions. However, as ionic strength increases further, strong attractive forces emerge in $U(r)$ and the kinetic arrest volume fraction shifts to lower volume fractions. This behavior is reminiscent of the re-entrant behavior seen in depletion attraction systems[44,45] and suggests that the weak attractions introduced by charge screening first results in greater mobility in dense suspensions of both particle shapes, but as the attractions become strong enough the tendency for kinetic arrest is enhanced corresponding to a gel or "attractive glass" nonequilibrium state and enhanced shear modulus. Note the very large reduction of the kinetic arrest volume fraction at the highest ionic strength of 1.0 M where $\phi_g \sim 0.36$ for both spheres and dicolloids. As is well known from prior theoretical and simulation studies (including our present calculations), the dense gel or attractive glass is characterized by a very short transient localization length controlled to leading order by the range of the attractive potential, in contrast to repulsive glasses where the localization length is larger and controlled by steric caging.[59]

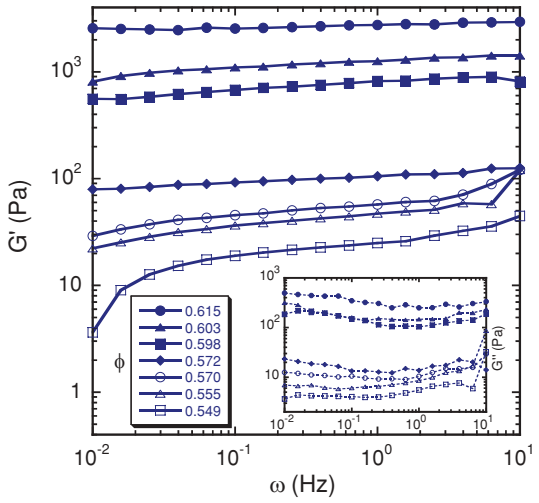

FIG. 4. $G'(\omega)$ for spheres at 0.03 M and volume fractions $>\phi_g$ demonstrating observance of a glassy plateau in the frequency range near 1 Hz. Inset shows $G''(\omega)$.

The qualitative change of increasing ionic strength on colloid dynamics is signaled by the "nose" of the kinetic arrest diagram corresponding to a maximal fluidic state. For both spheres and dicolloids this occurs at [I]$\sim$0.3 M, and the amount of enhancement of ϕ_g is $\sim$0.04–0.05 for both types of particles. Thus, although nonspherical particle shape dramatically delays kinetic arrest relative to the sphere, the effect of ionic strength on the interparticle interactions is similar for the two colloidal shapes.

We now employ the *a priori* computed interaction potentials in the CM version of the NMCT and NLE theories with RISM structural input to predict the behavior of

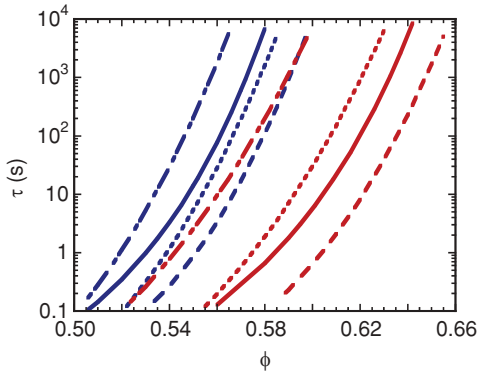

FIG. 6. $\tau(\phi)$ from NLE theory for S (blue) and sDC (red) at ionic strengths of 0.03 M (solid), 0.1 M (long dash), 0.5 M (short dash), and 1.0 M (dash-dot).

our experimental systems. The ideal MCT transition, or dynamic crossover, volume fractions, ϕ_c, are shown in Fig. 5 as the dashed curves, and numerical values are listed in Table II. The theoretical ϕ_c display all the same qualitative behavior as the experimental ϕ_g's, including the large enhancement for the nonspherical colloid and the nonmonotonic re-entrant behavior. Quantitatively, the computed ϕ_c are systematically smaller than their experimental kinetic arrest analogs. This trend has presumably two distinct origins. First, NMCT underpredicts ϕ_c compared to more sophisticated ideal MCT.[39,40] Second, and we believe more importantly, ϕ_c indicates only an onset or crossover volume fraction signaling the emergence of barriers and activated dynamics.[35,39,40]

The NLE theory at the CM level is now applied to compute the mean barrier hopping time, τ. Figure 6 shows the results as a function of volume fraction for spheres and dicolloids at four ionic strengths. Based on the known solvent viscosity, temperature, and particle size, τ_0 is computed to be 0.03 s for our system. For all the calculations we employ τ_s=0.1 s as a reasonable value that acknowledges the fact that $\tau_s/\tau_0>1$. Physically sensible adjustments of this value only shift computed kinetic volume fractions by ~0.01–0.02 at most since it enters as a prefactor. For all curves in Fig. 6, note the stronger than exponential growth of the relaxation time with ϕ. At fixed volume fraction, the barrier hopping time is much smaller for dicolloids than for spheres, and for both shapes varies nonmonotonically with ionic strength.

The kinetic arrest volume fractions, ϕ_g, are now computed using the results in Fig. 6 and the experimental criterion $\tau=2\pi$ s; analogous calculations are performed based on relaxation time criteria of 1 and 50 s in order to illustrate the sensitivity of the predictions to the arrest criterion adopted. The theoretical kinetic arrest boundaries are shown in Fig. 5. The agreement between experiment and theory is good (especially considering there are no adjustable parameters), and better for dicolloids, except for the highest ionic strength of 1.0 M. The theory predicts moderate particle shape anisotropy dramatically delays kinetic arrest, as well as the re-entrant form of the nonequilibrium boundary as the interparticle interaction changes from repulsive to attractive. Qualitatively, the kinetic arrest and dynamic crossover (NMCT) boundaries agree, although the "nose" feature is more developed for the latter. The theory strongly overpredicts the kinetic arrest volume fraction under high ionic strength conditions where attractive forces are likely dominant and possible quantitative errors in the attractive branch of $U(r)$ in Fig. 1 (discussed in Sec. III B) will have the largest consequences.

It should be noted that while particle polydispersity, surface roughness, and slight variations in experimental protocol may also contribute to the differences between experimental results and theory predictions, we have worked hard to create a system that conforms to the models used. Within our ability to characterize the system it appears to us that we have smooth hard core particles experiencing short range electrostatic repulsion and weak van der Waals attractions. The largest potential complication in comparing theory and experiment is likely quantitative inaccuracies of the interparticle potentials required as input to the structural and dynamical theories.

TABLE II. NMCT calculations of ϕ_c for the sphere (S) and symmetric dicolloid (sDC).

Ionic strength (M)	ϕ_c S	ϕ_c sDC
0.03	0.410	0.454
0.05	0.427	0.472
0.1	0.440	0.487
0.3	0.456	0.503
0.5	0.449	0.462
1.0	0.419	0.412

B. Additional theoretical analysis

A question of fundamental interest is the physical origin of the theoretical re-entrancy phenomenon for the present novel system of colloids interacting via soft Coulomb repulsions and van der Waals attractions. All dynamical predictions are ultimately determined by structure, the two most commonly discussed aspects being the static structure factor, $S_{ss}(k)$, and the pair correlation function, $g_{ss}(r)$. The dynamically relevant features of these correlations are on local scales, in particular $S_{ss}(k=k^*)$ where k^* is the wave vector of the cage scale maximum, and $g_{ss}(r=r^*)$, the "contact" value of the site–site interparticle radial distribution function. For the soft repulsion systems of present interest, the latter refers to the height of the first peak of the pair correlation function which does occur very close to r^*~D. This quantity can be thought of as quantifying a "sticky collision" rate or the strength/number of "physical bonds" between particles.[46]

Figure 7 presents calculations of these two structural quantities for the sphere and dicolloid as a function of ionic strength at two volume fractions, one representative of the dynamic crossover regime (0.45) and the other higher value representative of the kinetic arrest regime (0.6). The ionic strength trends are qualitatively identical at both volume fractions, and for both shapes. However, the contact value [Fig. 7(a)] and cage peak intensity [Fig. 7(b)] follow qualitatively opposite variations. The contact value monotonically increases with ionic strength, an intuitive trend since as at-

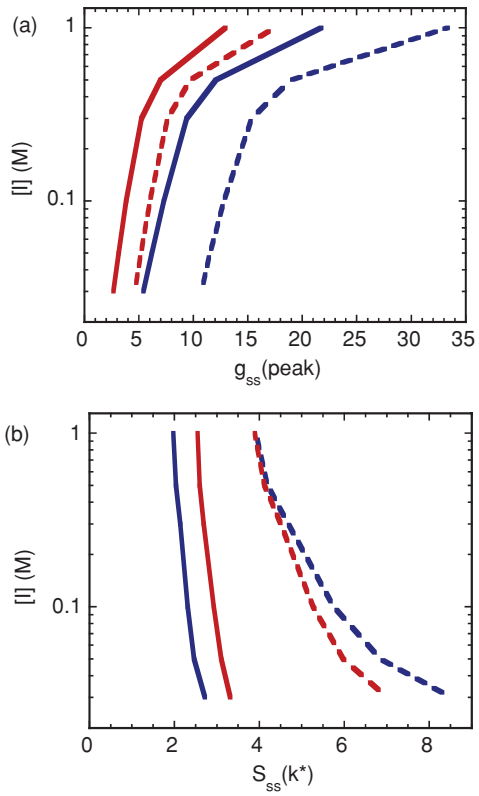

FIG. 7. RISM theory calculations of (a) the contact value of the site–site interparticle radial distribution function $g(r{=}D)$ and (b) the site–site static structure factor at the wave vector of the cage scale maximum $S(k{=}k^*)$ for S (blue) and sDC (red) as a function of ionic strength at volume fraction $\phi{=}0.45$ (solid) and $\phi{=}0.6$ (dash).

tractions are introduced one expects more contact particle clustering. However, $S_{ss}(k^*)$ monotonically decreases with attractions, a trend previously emphasized in the context of mixtures of nonadsorbing polymer and hard sphere colloids as "disordering" of cage constraints due to frustration between repulsive and attractive forces in determining first solvation shell coherence.[49,56,58] Note that for polymer-colloid depletion systems, $S_{ss}(k^*)$ is a nonmonotonic function of attraction strength (polymer concentration), and hence dynamical re-entrancy is interpreted at zeroth order solely in terms of cage coherence. This simple interpretation does not apply to our systems that interact via a more complex soft repulsion plus van der Waals attractions which are both modified as ionic strength is varied. Hence, we suggest the competition between attractive and repulsive forces that gives rise to the re-entrancy behavior reflects a competition between cage coherence effects and short range attraction driven contact aggregation.

The relaxation time calculations in Fig. 6 show a nonexponential growth and strong variation with ionic strength. A question of significant interest in both the thermal glass forming liquids[60] and colloidal suspensions[25,26,33,61] is how "dynamic fragility" depends on particle shape and interparticle forces. Fragility is a scalar quantification of how rapidly a relaxation time grows with a control parameter, typically temperature or volume fraction. Figure 8 replots the theoretical results in Fig. 6 in a doubly normalized manner that defines fragility. Overall, the fragility initially increases modestly with ionic strength for both spheres and dicolloids in an almost identical fashion, and then becomes roughly invariant to [I] at the higher ionic strengths.

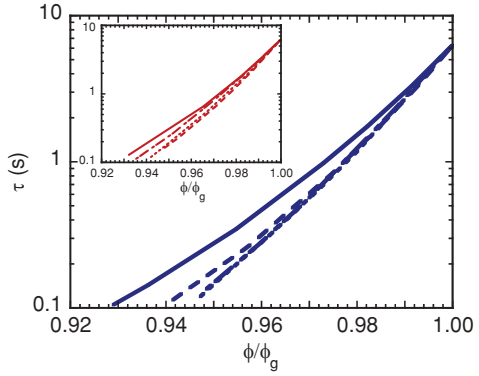

FIG. 8. Fragility plot of the theoretical mean hopping time calculations for S (blue), sDC (red). Ionic strengths: 0.03 M (solid), 0.1 M (long dash), 0.5 M (short dash), and 1.0 M (dash-dot).

C. Shear elasticity

The mechanical experiments allow measurement of the elastic shear modulus as a function of volume fraction, ionic strength, and particle shape, which can be quantitatively compared to NMCT predictions. Figure 9 shows the experimental G'^* (shear modulus rendered dimensionless by either D^3/kT in the case of spheres, or L^2D/kT for dicolloids)[19] as a function of volume fraction in a log-linear format. At each ionic strength, G' for the dicolloids lies below that of the spheres, and shifts nonmonotonically with [I], as expected from the kinetic arrest diagram. All moduli grow roughly exponentially with volume fraction, with slopes that weakly increase at high ionic strengths, and which are always somewhat smaller for dicolloids. Interestingly, the apparent shift in slope seems largest for the ionic strength corresponding to the "nose" of

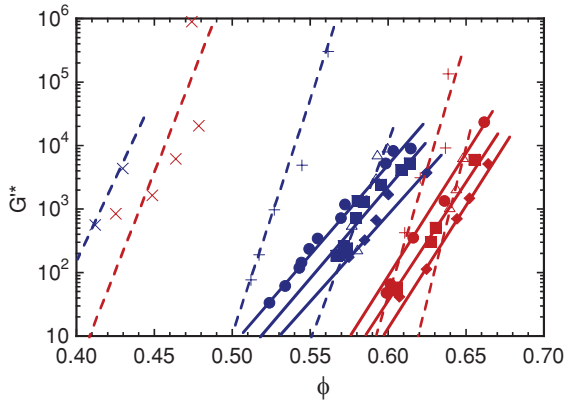

FIG. 9. Measured low shear rate dimensionless elastic modulus of spheres (blue) and dicolloids (red) at ionic strengths of 0.03 (circles), 0.05 (squares), 0.1 (diamonds), 0.3 (open triangles), 0.5 (plus), 1.0 (x's). Lines are drawn to guide the eye to each set of data at a single ionic strength. Solid lines/closed points represent repulsive conditions, while dashed lines/open points represent attractive conditions.

the nonequilibrium phase diagram[44,56] where attractive and repulsive forces are most balanced.

Previous theoretical work[19,21,22] predicted that for uniaxial particles experiencing hard core interactions, rescaling the volume fraction based on the distance from the dynamic crossover, ϕ/ϕ_c-1, and shear modulus based on the thermal energy per colloid volume results in collapse of the modulus data for different particle shapes. Since we cannot measure ϕ_c experimentally, the NMCT predictions for ϕ_c are employed. The experimental data in Fig. 9 are replotted in this doubly normalized manner in Fig. 10, and the corresponding theoretical calculations are also shown. The theoretical results for spheres and dicolloids do nearly collapse, but onto curves that change systematically with ionic strength. Experiments behave in a similar manner for repulsive colloids, although the apparent slope of the roughly exponential dependence is larger than predicted. However, for attractive particles the collapse fails, although the shear modulus is largest at high ionic strengths in qualitative accord with theory. The origin of the deviations between theory and experiment in Fig. 10 is not clear, but errors incurred by the RISM structural input at very high volume fractions, and possible quantitative inaccuracies to the pair potential for strongly attractive particles, are two plausible candidates.

Since the sphere and dicolloid experimental data from the three lower ionic strengths superimpose well, as predicted previously only for hard interactions,[19,43] these systems can be considered "effectively hard" colloids characterized by an effective larger diameter due to the electrostatic repulsion. The latter is determined based on a surface-to-surface distance, δ, where the particles experience a pair repulsion of magnitude $1kT$, and hence $D_{\text{eff}}=D+\delta$, $L_{\text{eff}}=L+\delta$, and $\phi_{\text{eff}}=\phi(1+\delta)^3$. The rescaled volume fraction of the effective hard core systems is then $(\phi_{\text{eff}}/\phi_c^H-1)$, where ϕ_c^H is the dynamic crossover volume fraction. The result of replotting the repulsive colloid shear modulus data in this manner is shown in Fig. 11, along with the corresponding NMCT predictions for all hard dicolloids which are identical for spheres and dicolloids in this representation. Indeed, we find that all data points fall nearly on the same curve thus confirming the idea that our net repulsive colloids which interact via screened electrostatic repulsions and truncated van der Waals attractions can be modeled as effectively hard.

In many ways the collapse of the shear modulus data obtained by rescaling the volume fraction is similar to results from gel systems where data collapses are achieved by scaling on the gel transition volume fraction.[61] However, in the present case, the collapse is predicted by the theory as a consequence of the direct connection between r_{loc}, ϕ/ϕ_c, and the shear modulus as discussed in detail in Refs. 19 and 48.

D. Summary of experiment-theory confrontation

The new experimental results presented above confirm four major predictions of the MCT and NLE theories: (1) the re-entrant shape of the kinetic arrest diagram, (2) the strong enhancement of the arrest volume fraction by modest colloidal anisotropy, (3) the effect of ionic strength on the elastic shear modulus, and (4) the collapse of the modulus data under effectively hard conditions when volume fraction is scaled on $(\phi_{\text{eff}}/\phi_c^H)-1$. However, the dependence of G'^* on (reduced) volume fraction has *not* been confirmed, and the theory significantly underpredicts the slope of the exponential dependence of the elastic modulus on volume fraction. Besides the issues of the accuracy of the structural and dynamical approximations of the theory, and uncertainties in the computed interparticle potentials, we note the theoretical measure of relaxation is a mean barrier hopping time and the shear modulus is computed under fully localized conditions. These latter two idealizations presumably also incur some errors given the experiments measure a mechanically determined relaxation time from frequency dependent moduli. It would be interesting to extend the shear modulus experiments to higher measurement frequencies where the material is expected to better approximate an ideal solid response, but this is not feasible due to instrumental limitations.

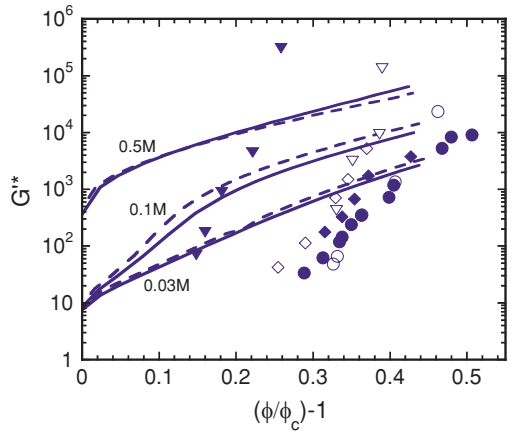

FIG. 10. G'^* ($G'^*=G'D^3/kT$ or $G'L^2D/kT$) as a function of reduced volume fraction for spheres (closed points) and dicolloids (open points) at ionic strengths of 0.03 (circles), 0.1 (diamond), and 0.5 M (triangles). Curves indicate the corresponding NMCT predictions for spheres (solid) and dicolloids (dash).

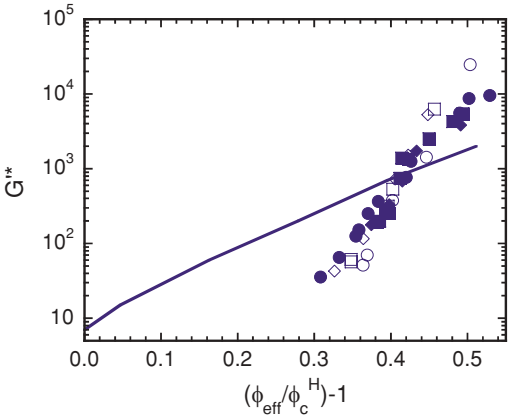

FIG. 11. G'^* ($G'^*=G'D^3/kT$ or $G'L^2D/kT$) as a function of reduced *effective* volume fraction for only repulsive conditions: 0.03 (circles), 0.05 M (squares), 0.1 (diamonds). All ionic strengths and particle shapes collapse onto a single universal curve. Hard particle theory is shown as a solid curve.

V. CONCLUSION

We have designed a new experimental colloidal system to probe how the weak shape anisotropy of uniaxial particles, and variable repulsive and attractive interparticle forces, impact slow dynamics, shear elasticity, and kinetic vitrification in dense suspensions. The introduction of shape anisotropy dramatically delays the onset of glass formation, as predicted theoretically. Tuning the particle interaction from repulsive, to near hard, to attractive reveals re-entrant phase behavior. While re-entrant phase behavior has been demonstrated for hard sphere colloid plus nonadsorbing polymer entropic depletion system,[44,45] this is the first study of particles that interact via attractive van der Waals forces and a soft electrostatic repulsion. Hence, our observations demonstrate the reentrancy phenomenon is more general and applies to spherical colloids interacting via different forces, and also nonspherical particles.

The systems created and studied in this work have potentially several interesting applications in materials science and engineering. For example, a practical new strategy is suggested in the search for flowable, ultrahigh volume fraction suspensions based on modestly nonspherical colloids that interact via weak attractions, two features that combine to produce a remarkably large widening of the fluid state. Moreover, such systems may find use as responsive fluids which can be reversibly switched between a fluid and gel, or a fluid and glass, states of highly diverse and tunable elasticity based on *in situ* modification of the suspension ionic strength.

Interesting future directions include: (i) direct experimental probe (perhaps by confocal microscopy[62]) of the trajectories of nonspherical particles under dense fluid, glass, and gel conditions; (ii) the role of particle shape and coupled translational-rotational dynamics on nonlinear yielding of colloidal glasses and gels;[63] and (iii) the structure, viscoelasticity, and kinetic arrest of nonspherical Janus colloids[64] with controllable chemical heterogeneity. These problems are presently under active experimental and theoretical study.

ACKNOWLEDGMENTS

Our work is supported by the U.S. Department of Energy, Division of Materials Sciences under Award No. DE-FG02-07ER46471, through the Frederick Seitz Materials Research Laboratory (FS-MRL) at the University of Illinois. Experiments were carried out in part in the FS-MRL Central Facilities which are partially supported by the U.S. Department of Energy under Grant Nos. DE-FG02-07ER46453 and DE-FG02-07ER46471.

[1] E. Bianchi, J. Largo, P. Tartaglia, E. Zaccarelli, and F. Sciortino, Phys. Rev. Lett. **97**, 168301 (2006).
[2] F. Sciortino, E. Bianchi, J. F. Douglas, and P. Tartaglia, J. Chem. Phys. **126**, 194903 (2007).
[3] Z. L. Zhang and S. C. Glotzer, Nano Lett. **4**, 1407 (2004).
[4] S. C. Glotzer and M. J. Solomon, Nature Mater. **6**, 557 (2007).
[5] V. N. Manoharan, M. T. Elsesser, and D. J. Pine, Science **301**, 483 (2003).
[6] D. Dendukuri, K. Tsoi, T. A. Hatton, and P. S. Doyle, Langmuir **21**, 2113 (2005).
[7] T. Fujibayashi and M. Okubo, Langmuir **23**, 7958 (2007).
[8] J.-W. Kim, R. Larsen, and D. A. Weitz, Adv. Mater. **19**, 2005 (2007).
[9] E. B. Mock, H. De Bruyn, B. Hawkett, R. Gilbert, and C. F. Zukoski, Langmuir **22**, 4037 (2006).
[10] H. Sheu, M. El-Aasser, and J. Vanderhoff, J. Polym. Sci., Part A: Polym. Chem. **28,** 653 (1990).
[11] E. Snoeks, A. van Blaaderen, T. van Dillen, C. M. van Kats, M. L. Brongersma, and A. Polman, Adv. Mater. **12**, 1511 (2000).
[12] S. M. Yang, S. H. Kim, J. M. Lim, and G. R. Yi, J. Mater. Chem. **18**, 2177 (2008).
[13] D. Zerrouki, B. Rotenberg, S. Abramson, J. Baudry, C. Goubault, F. Leal-Calderon, D. J. Pine, and M. Bibette, Langmuir **22**, 57 (2006).
[14] K. M. Keville, E. I. Franses, and J. M. Caruthers, J. Coll. Inter. Sci. **144**, 103 (1991).
[15] A. van Blaaderen, Nature **439**, 545 (2006).
[16] S.-H. Chong and W. Götze, Phys. Rev. E **65**, 041503 (2002).
[17] W. Götze and L. Sjörgen, Rep. Prog. Phys. **55**, 241 (1992).
[18] S.-H. Chong, A. J. Moreno, F. Sciortino, and W. Kob, Phys. Rev. Lett. **94**, 215701 (2005).
[19] G. Yatsenko and K. S. Schweizer, J. Chem. Phys. **126**, 014505 (2007).
[20] R. Zhang and K. S. Schweizer, Phys. Rev. E **80**, 011502 (2009).
[21] G. Yatsenko and K. S. Schweizer, Phys. Rev. E **76**, 041506 (2007).
[22] G. Yatsenko and K. S. Schweizer, Langmuir **24**, 7474 (2008).
[23] M. Letz, R. Schilling, and A. Latz, Phys. Rev. E **62**, 5173 (2000).
[24] C. DeMichelle, R. Schilling, and F. Sciortino, Phys. Rev. Lett. **98**, 265702 (2007).
[25] M. Tripathy and K. S. Schweizer, J. Chem. Phys. **130**, 244907 (2009).
[26] M. Tripathy and K. S. Schweizer, J. Chem. Phys. **130**, 244906 (2009).
[27] A. Donev, I. Cisse, D. Sachs, E. A. Variano, F. H. Stillinger, R. Connelly, S. Torquato, and P. M. Chaikin, Science **303**, 990 (2004).
[28] S. R. Williams and A. P. Philipse, Phys. Rev. E **67**, 051301 (2003).
[29] S. Sacanna, L. Rossi, A. Wouterse, and A. P. Philipse, J. Phys.: Cond. Matt. **19**, 376108 (2007).
[30] F. Ozon, G. Petekidis, and D. Vlassopoulos, Ind. Eng. Chem. Res. **45**, 6946 (2006).
[31] J. R. Seth, M. Cloitre, and R. T. Bonnecaze, J. Rheol. **50**, 353 (2006).
[32] Z. Zhang, N. Xu, D. Chen, P. Yunker, A. M. Alsayed, K. B. Aptowicz, P. Habdas, A. J. Liu, S. R. Nagel, and A. G. Yodh, Nature **459**, 83 (2009).
[33] J. Mattson, H. M. Wyss, A. Fernando-Nieves, K. Miyazaki, Z. Hu, D. R. Reichman, and D. A. Weitz, Nature **462**, 83 (2009).
[34] W. R. Chen, F. Mallamace, C. J. Glinka, E. Fratini, and S. H. Chen, Phys. Rev. E **68**, 041402 (2003).
[35] K. S. Schweizer, Curr. Opin. Coll. Inter. Sci. **12**, 297 (2007).
[36] S. K. Kumar, G. Szamel, and J. F. Douglas, J. Chem. Phys. **124**, 214501 (2006).
[37] Y. Brumer and D. R. Reichman, Phys. Rev. E **69**, 041202 (2004).
[38] G. Brambilla, D. El Masri, M. Pierno, L. Berthier, L. Cipelletti, G. Petekidis, and A. B. Schofield, Phys. Rev. Lett. **102**, 085703 (2009).
[39] K. S. Schweizer and E. J. Saltzman, J. Chem. Phys. **119**, 1181 (2003).
[40] K. S. Schweizer, J. Chem. Phys. **123**, 244501 (2005).
[41] E. J. Saltzman and K. S. Schweizer, J. Chem. Phys. **119**, 1197 (2003).
[42] T. R. Kirkpatrick and P. G. Wolynes, Phys. Rev. A **35**, 3072 (1987).
[43] R. C. Kramb, R. Zhang, K. S. Schweizer, and C. F. Zukoski, Phys. Rev. Lett. **105**, 055702 (2010).
[44] W. C. K. Poon, J. Phys.: Cond. Matt. **14**, R859 (2002).
[45] K. N. Pham, A. M. Puertas, J. Bergenholtz, S. U. Egelhaaf, A. Moussaid, P. N. Pusey, A. B. Schofield, M. E. Cates, M. Fuchs, and W. C. K. Poon, Science **296**, 104 (2002).
[46] D. Chandler and H. C. Andersen, J. Chem. Phys. **57**, 1930 (1972).
[47] J.-P. Hansen and I. R. McDonald, Theory of Simple Liquids, 3rd ed. (Academic, New York, 2006).
[48] K. S. Schweizer and G. Yatsenko, J. Chem. Phys. **127**, 164505 (2007).
[49] Y.-L. Chen and K. S. Schweizer, J. Chem. Phys. **120**, 7212 (2004).
[50] K. S. Schweizer and E. J. Saltzman, J. Phys. Chem. B **108**, 19729 (2004).
[51] S. J. Partridge, Ph.D. thesis, Bristol University, 1985.
[52] Accounting for short range Coulomb repulsions allows us to define an effective hard core volume fraction: $\phi_{\rm eff} = \phi(V^*_{\rm eff}/V^*)$, where $V^*_{\rm eff}$ is: $(D_{\rm eff})^3$ and $D_{\rm eff}L_{\rm eff}^2$ where $D_{\rm eff} = D+\Delta$ and $L_{\rm eff} = L+\Delta$, for spheres and homonuclear dicolloids, respectively.
[53] E. B. Mock and C. Zukoski, J. Rheol. **51**, 541 (2007).
[54] I. M. Krieger, Adv. Coll. Inter. Sci. **3**, 111 (1972).
[55] V. Gopalakrishnan and C. F. Zukoski, Ind. Eng. Chem. Res. **45**, 6906 (2006).

[56]K. A. Dawson, Curr. Opin. Coll. Inter. Sci. **7**, 218 (2002).
[57]J. Bergenholtz and M. Fuchs, Phys. Rev. E **59**, 5706 (1999).
[58]J. Bergenholtz, W. C. K. Poon, and M. Fuchs, Langmuir **19**, 4493 (2003).
[59]E. Zaccarelli and W. C. K. Poon, Proc. Natl. Acad. Sci. U.S.A., **106**, 15203 (2009).
[60]C. A. Angell, K. L. Ngai, G. B. McKenna, P. F. McMillan, and S. W. Martin, J. App. Phys. **88**, 3113 (2000).
[61]S. Ramakrishnan and C. F. Zukoski, Langmuir **22**, 7833 (2006).
[62]E. R. Weeks and D. A. Weitz, J. Chem. Phys. **284**, 361 (2002).
[63]A. Wierenga, A. P. Philipse, H. N. W. Lekkerkerker, and D. V. Boger, Langmuir **14**, 55 (1998).
[64]S. Jiang, Q. Chen, M. Tripathy, E. Luijten, K. S. Schweizer, and S. Granick, Adv. Mater. **22**, 1060 (2010).
[65]Z. Cheng, J. Zhu, P. M. Chaikin, S.-E. Phan, and W. B. Russel, Phys. Rev. E **65**, 041405 (2002).